Ensuring Profitability of Energy Storage

Y. Dvorkin, *Student Member*, *IEEE*, R. Fernández-Blanco, *Member*, *IEEE*, D. S. Kirschen, *Fellow*, *IEEE*, H. Pandžić, *Member*, *IEEE*, J.-P. Watson, *Member*, *IEEE*, and C. A. Silva-Monroy, *Member*, *IEEE*

***Abstract*—Energy storage (ES) is a pivotal technology for dealing with the challenges caused by the integration of renewable energy sources. It is expected that a decrease in the capital cost of storage will eventually spur the deployment of large amounts of ES. These devices will provide transmission services, such as spatiotemporal energy arbitrage, i.e., storing surplus energy from intermittent renewable sources for later use by loads while reducing the congestion in the transmission network.**

This paper proposes a bilevel program that determines the optimal location and size of storage devices to perform this spatiotemporal energy arbitrage. This method aims to simultaneously reduce the system-wide operating cost and the cost of investments in ES while ensuring that merchant storage devices collect sufficient profits to fully recover their investment cost. The usefulness of the proposed method is illustrated using a representative case study of the ISO New England system with a prospective wind generation portfolio.

***Index Terms*—Bilevel optimization, distributed energy storage, energy storage investment, energy storage profitability, power system economics, power system planning, storage siting, storage sizing, wind power generation.**

NOMENCLATURE

A. Sets and Indices

B	Set of buses, indexed by b.
E	Set of representative days, indexed by e.
I, I_b	Set of conventional generators and subset of conventional generators connected to bus b, indexed by i.
J	Set of ES blocks, indexed by j.
L	Set of transmission lines, indexed by l.
T	Set of time intervals, indexed by t.
Ξ_{UL}	Set of upper-level (UL) decision variables.
$\Xi_{\text{PLL/DLL}}$	Set of primal/dual lower-level (PLL/DLL) decision variables.
k	Auxiliary index of time intervals.
$o(l), r(l)$	Indices of the sending and receiving buses of transmission line l.

Manuscript received October 19, 2015; revised March 1, 2016; accepted May 2, 2016.

This work was supported in part by the ARPA-E Green Electricity Network Integration (GENI) program under project DE-FOA-0000473 and U.S. Department of Energy's National Nuclear Security Administration under Contract DE-AC04-94AL85000.

Yury Dvorkin, Ricardo Fernández-Blanco, and Daniel S. Kirschen are with the Department of Electrical Engineering, University of Washington, Seattle, WA, USA, 98195-2500 (e-mails: dvorkin@uw.edu, rfbc85@uw.edu, and kirschen@uw.edu).

Hrvoje Pandžić is with the Faculty of Electrical Engineering and Computing University of Zagreb, Zagreb HR-10000, Croatia (e-mail: hrvoje.pandzic@ieee.org). His work has been supported in part by Croatian Science Foundation and Croatian TSO (HOPS) under the project I-2538-2015.

Jean-Paul Watson and Cesar A. Silva-Monroy are with the Sandia National Laboratories, Albuquerque, NM 87185-1320 USA (e-mails: jwatson@sandia.gov and casilv@sandia.gov).

B. Continuous Variables

$a^1_{e,t,b,j}, a^{2,\text{ch/dis}}_{e,t,b,j}$	Auxiliary variables used for linearization.
$ch_{e,t,b}, dis_{e,t,b}$	ES charging and discharging rate at bus b during time interval t on representative day e, MW.
$eSoC_{e,t,b}$	State-of-charge of ES at bus b at the end of time interval t on representative day e, MWh.
$eSoC^{\max}_b$	Maximum state-of-charge of the ES at bus b, MWh.
$f_{e,t,l}$	Power flow in transmission line l during time interval t on representative day e, MW.
$g_{e,t,i}$	Output of conventional generator i during time interval t on representative day e, MW.
$\underline{h}_{e,t,i}, \overline{h}_{e,t,i}$	Auxiliary variables used for linearization.
IC	Investment cost, \$.
$OC^{\text{PLL/DLL}}_e$	Objective function of the PLL/DLL problem on representative day e, \$.
$p^{\max}_b$	Maximum power rating of ES at bus b, MW.
$ws_{e,t,b}$	Wind spillage at bus b during time interval t on representative day e, MW.
$\theta_{e,t,b}$	Voltage phase angle at bus b during time interval t on representative day e, rad.

C. Dual Continuous Variables

Dual variables associated with the PLL problem constraints:

$\underline{\alpha}_{e,t,i}, \overline{\alpha}_{e,t,i}$	Min/max power output of conventional generators, eq. (11).
$\beta^{RD/RU}_{e,t,i}$	Ramp down/up limit of conventional generators, eq. (12).
$\xi_{e,t,l}$	Power flow, eq. (13).
$\underline{\delta}_{e,t,l}, \overline{\delta}_{e,t,l}$	Power flow limits, eq. (14).
$\epsilon_{e,t,b}$	State-of-charge of ES, eq. (15).
$\overline{\varphi}^{\text{ch/dis}}_{e,t,b}$, $\underline{\varphi}^{\text{ch/dis}}_{e,t,b}$	Charging/discharging limits of ES, eq. (16)–(17).
$\overline{\varphi}^{\text{eSoC}}_{e,t,b}$, $\underline{\varphi}^{\text{eSoC}}_{e,t,b}$	State-of-charge limits of ES, eq. (18).
$\lambda_{e,t,b}$	Nodal power balance, eq. (19).
$\gamma_{e,t,b}$	Upper bound on the wind spillage, eq. (20).

D. Binary Variables

$u_{b,j}$	Binary variable corresponding to the placement decision of ES block j at bus b.
$v_{e,t,i}$	On/off status of conventional generator i during time interval t on representative day e.
$y_{e,t,i}$, $z_{e,t,i}$	Start-up and shutdown status of conventional generator i during time interval t on representative day e.

E. Parameters

c^{eSoC}, c^{p}	Capital cost of ES per MWh ($/MWh) and per MW ($/MW).
c_i^{g}	Incremental cost of conventional generator i, $/MWh.
c_i^{nlc}	No-load cost of conventional generator i, $.
c_i^{start}	Start-up cost of conventional generator i, $.
$d_{e,t,b}$	Demand at bus b during time interval t on representative day e, MW.
DT_i, UT_i	Minimum down- and up-time of conventional generator i, h.
$\overline{F}_l$	Maximum power flow in transmission line l, MW.
$\overline{G}_i, \underline{G}_i$	Maximum and minimum power output of conventional generator i, MW.
$G_{e,i}^0$	Initial power output of conventional generator i on representative day e, MW.
$IC^{\max}$	Investment budget, $.
$\overline{L}_{e,i}$, $\underline{L}_{e,i}$	Number of hours that conventional generator i must remain on/off at the beginning of representative day e. Note that if $\overline{L}_{i,e} \neq 0$, then $\underline{L}_{i,e} = 0$, and vice versa.
M	Sufficiently large positive number.
n_B	Number of buses.
n_E	Number of representative days.
n_I	Number of conventional generators.
n_J	Number of ES blocks.
n_L	Number of transmission lines.
n_T	Number of time intervals.
RU_i,RD_i	Ramp up and down of conventional generator i, MW/h.
$u_b^{\max}$	Maximum number of ES blocks that can be installed at bus b.
$VoWS$	Value of wind spillage, $/MWh.
$V_{e,i}^0$	Initial commitment of conventional generator i on representative day e.
$w_{e,t,b}^{\text{f}}$	Wind power forecast at bus b during time interval t on representative day e, MW.
x_l	Reactance of transmission line l.
$\bar{\lambda}_{e,t,b}$	Locational marginal price (LMP) from the no-ES case, $/MWh.
ω_e	Weight of representative day e.
ρ	Energy-to-power ratio of ES, h.
χ	Parameter relating the investment cost of ES and their expected profit.
$\Delta eSoC$	Energy rating of the single ES block, MWh.
$\Delta\lambda$	Parameter modeling the deviation of the LMP from the no-ES case.
$\Delta\tau$	Duration of time interval t, h.
$\aleph^{\text{ch/dis}}$	Charging/discharging efficiency of ES.

I. Introduction

Recent advances in material science make the large-scale deployment of electrochemical energy storage (ES) in the transmission system a technically feasible option [1]. Applications such as spatiotemporal energy arbitrage [2], peak shaving [3], frequency [4] and voltage [5] support, as well as congestion management [2], [6] have been proposed. Provided anticipated capital cost reductions and increased charging/discharging efficiencies are achieved, system operators (SOs) could use grid-scale electrochemical ES distributed in the transmission network to facilitate the reliable integration of uncertain and variable renewable generation [7]. For instance, Solomon *et al.* [8] estimate that the state of California will need 186 GWh/22 GW of ES to enable an approximately 85% penetration of renewable generation. However, the authors intentionally avoid discussing the economic implications of such large-scale ES deployment due to the uncertainty of the capital costs. Kintner-Meyer *et al.* [9] conclude that the Northwest Power Pool will need up to 10 GWh/1 GW of ES resources by 2019 to be able to balance 14.4 GW of installed wind generation capacity. However, the economic analysis in [9] also reveals that revenue streams for such a deployment of ES are expected to be thin.

Regulators and SOs acknowledge that although the deployment of ES can reduce the cost of operating the grid, for-profit owners of ES should collect sufficient profit to justify their investments [10], [11]. For instance, the CAISO roadmap for ES prioritizes the challenge of '*realize(-ing) the full revenue opportunities consistent with the value ES can provide*' [10]. In line with [10] and FERC Order No. 792 [11], this paper shows how both the system-wide cost savings and the profits collected by ES owners can be accounted for while *jointly* optimizing ES siting and sizing decisions for spatiotemporal arbitrage. This joint optimization is necessary because, unlike pumped-hydro plants that can only be installed in a limited number of locations, electrochemical ES can be distributed more widely in the transmission network [2], [8], [10].

The complexity of joint siting and sizing of ES arises from the need to balance long- and short-term costs and benefits [2], as well as from the difficulties associated with taking transmission constraints into account [12]. In [13], the value of ES siting and sizing is itemized for different storage technologies and grid services. Based on their numerical studies, the authors of [13] conclude that ignoring levelizing short- and long-term benefits of ES and tranmission constraints leads to an inaccurate assessment of the value of ES. To overcome this complexity, Dvijotham *et al.* [14] and Pandžić *et al.* [2] use sampling-based approaches, which site and size ES providing spatiotemporal energy arbitrage for each day of the year separately. To aggregate the daily decisions in the preferable ES locations and sizes, Dvijotham *et al.* [14] analyze the daily frequency of the siting and sizing using a heuristic greedy algorithm. Similarly, Pandžić *et al.* [2] select the preferred locations of ES based on their daily frequency over the course of the year and compute the optimal size of ES at every bus as the average of the daily sizing decisions. Makarov *et al.* [4] limit the application of ES to providing balancing services and aggregate the Western Electricity Coordinating Council system to a one-bus model. In [4], the ES ratings for various timescales are computed by performing a Discrete Fourier Transform on the balancing power profile. Unlike [2], [13], [14], the approach in [4] does not consider economic factors and, thus, calculates the maximum physical limit of ES deployment that could be theoretically installed.

The common thread of [2], [4], [9], [13], [14] is that ES is installed solely to minimize the system-wide operating cost. However, in practice ES is likely to be owned by independent entities that aim to maximize their profits [15]. These ES devices are therefore likely to be scheduled differently from those in [2], [4], [13], [14], thus affecting the cost savings that the SO might achieve from their deployment. Wogrin *et al.* [12] and Castillo *et al.* [16] co-optimize the system-wide operating cost and the operating cost of ES. As shown in [16], minimizing the system-wide operating cost in a convex economic dispatch formulation also yields the maximum profit for ES owners in a perfectly competitive market. However, binary commitment decisions on conventional generators and their minimum up and down time constraints are neglected in [16]. This approach may therefore yield inaccurate ES siting and sizing decisions. Finally, the models in [12], [16] do not guarantee that the maximized ES profit will be sufficient to fully recover the investments made by ES owners.

This paper proposes a computationally tractable bilevel program (BP) to optimize ES siting and sizing decisions in a meshed transmission network considering the perspective of both the SO and ES owners. The main contributions are as follows:

1) As in [2], [12]–[14], [16], the proposed BP jointly sites and sizes ES used for spatiotemporal energy arbitrage to minimize the system-wide operating cost and the ES investment cost. Unlike in [2], [12]–[14], [16], the proposed BP explicitly accounts for the ES profit collected from the electricity market. Finally, unlike in [12], [16], it also accommodates the binary nature of commitment decisions on conventional generators.
2) Additionally, the bilevel structure of the model makes it possible to compute endogenously locational marginal prices (LMPs), which can be used to relate explicitly the investment cost of ES and their expected profit as well as to study the ability of ES to influence LMPs. Thus, the proposed BP accounts for the mutual dependency between investment decisions on ES and LMPs. The relationship between the investment cost and expected profit is then enforced by a minimum expected profit constraint ensuring that the ES profits are sufficient to recover the investment costs.
3) The resulting profit-constrained BP gives rise to a nonlinear problem since the ES profit is formulated as a nonlinear expression. This work presents a duality-based approach to equivalently transform the proposed BP into a nonlinear equivalent and a novel linearization scheme that makes it possible to reformulate it as an equivalent mixed-integer linear programing (MILP) problem.
4) The proposed approach is applied to a test-bed of the ISO New England system [17] with off-the-shelf software. The case study analyzes the impact of the profit constraint on the ES siting and sizing decisions, the SO operating cost and savings, and the ES profits. The sensitivity of these decisions is analyzed for different investment budgets, operating strategies, and ES capital cost scenarios. The numerical results presented in this paper demonstrate the usefulness of this approach for regulators and SOs in assessing the economic viability of the ES deployment by balancing the SO cost savings and ES owner profits.

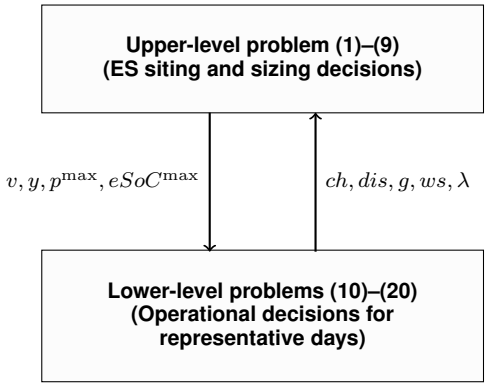

Fig. 1. An illustration of the proposed bilevel program and the interfaces between the upper- and lower-level problems. For the sake of clarity the indices of the decision variables have been omitted.

The remainder of this paper is organized as follows. In Section II the proposed BP is formulated. In this BP, typical scheduling and dispatch constraints on conventional and wind generators are combined with new investment and expected profit constraints on merchant ES. Section III describes the duality-based solution technique [18]. Section IV presents the experimental setup and compares different siting and sizing decisions obtained with the proposed BP in terms of the SO operating cost and savings as well as ES investments and profits. Section V presents the conclusions and outlines the needs for further research.

II. Problem Formulation

The proposed BP consists of an upper-level (UL) and a lower-level (LL) problem, as shown in Fig. 1. The UL problem minimizes the expected system-wide operating cost over all representative days and the investment cost of the profit-constrained ES siting and sizing decisions. A separate LL problem is formulated for each representative day to compute the least-cost system-wide operating cost subject to the operational constraints and conditions for that day. As explained in [18], this BP can be solved using the duality-based solution technique that requires the convexity of the LL problems. Therefore, as in [19]–[21], the constraints on binary decisions, e.g., the on/off statuses of conventional generators, are enforced in the UL problem and the corresponding binary decisions parametrize the LL problems.

Fig. 1 shows that the ES ratings ($p_b^{\max}$ and $eSoC_b^{\max}$) and binary decisions on generators ($v_{e,t,i}$ and $y_{e,t,i}$) resulting from the UL problem affect the decisions made in the LL problems. Similarly, the dispatch decisions ($g_{e,t,i}$ and $ws_{e,t,b}$) and the ES charging/discharging decisions ($ch_{e,t,b}$ and $dis_{e,t,b}$) resulting from the LL problems affect the decisions made in the UL problem. The LL problems yield LMPs ($\lambda_{e,t,b}$), which, in turn, are used in the UL problem to compute the profit collected by the ES owners.

A. Upper-Level Problem

The UL objective function is:

$$\min_{\Xi_{\text{UL}}} \sum_{e\in E} \left(\omega_e \cdot OC_e^{\text{PLL}}\right) + IC, \tag{1}$$

where OC_e^{PLL} is the system-wide operating cost as defined in (10) and $\Xi_{\text{UL}} = \{IC, p_b^{\max}, SoC_b^{\max}, v_{e,t,i}, y_{e,t,i}, z_{e,t,i}\}$ are the UL decision variables. The first term in (1) represents the operating cost over all representative days, OC_e^{PLL}, calculated using the weighing factor ω_e of each representative day e. The second term in (1) represents the investment cost resulting from the ES siting and sizing decisions. The UL constraints are as follows:

1) Investment constraints: To balance modeling accuracy and computational complexity, the investment model is assumed to be static, i.e., all investment decisions are optimized for operations during a given target year in the future [22]. Thus, the investment cost is computed as in [2] using the ES ratings ($p_b^{\max}$ and $eSoC_b^{\max}$) and daily prorated per MWh and MW capital costs (c^{eSoC} and c^{P}):

$$IC = \sum_{b\in B} \left(c^{\text{eSoC}} \cdot eSoC_b^{\max} + c^{\text{P}} \cdot p_b^{\max}\right), \tag{2}$$

$$IC \le IC^{\max}, \tag{3}$$

where parameters c^{eSoC} and c^{P} are calculated based on the net present value approach and assuming no depreciation of installed ES. Note that depreciation can be factored in parameters c^{eSoC} and c^{P}, as explained in [23], if decision-makers have a reasonable estimate of the residual worth of installed ES. In addition, constraint (3) imposes the budget limit on the total investment cost.

2) Profit constraint: ES owners pay or get paid the LMP ($\lambda_{e,t,b}$) when they charge or discharge their units. Therefore, the expected profit of an ES owner over the representative days is related to the investment cost by the following constraint:

$$\sum_{e\in E} \omega_e \cdot \sum_{b\in B}\sum_{t\in T} \lambda_{e,t,b} \cdot \left(dis_{e,t,b} \cdot \aleph^{\text{dis}} - ch_{e,t,b}/\aleph^{\text{ch}}\right) \ge \chi \cdot IC. \tag{4}$$

In (4), parameter χ can be viewed as a rate of return that the ES owner anticipates to receive from investment IC [24]. This parameter can be set by investors according to their profitability preferences. If $\chi \ge 1$, the expected profit in the left-hand side of (4) is sufficient for the investor to fully recover the investment cost, including energy losses due to $\aleph^{\text{dis/ch}} < 1$. Therefore, (4) precludes siting and sizing decisions that would result in insufficient profit opportunities[1], which is a significant improvement over the techniques described in [2], [12]–[14], [16].

Mathematically, $\lambda_{e,t,b}$ in (4) is a LL dual variable associated with constraint (19) and, therefore, the left-hand side of (4) contains two nonlinear products of the LL dual and primal decision variables ($\lambda_{e,t,b} \cdot dis_{e,t,b}$ and $\lambda_{e,t,b} \cdot ch_{e,t,b}$). Appendix A-1 presents a novel linearization scheme, which reformulates (4) as an equivalent linear constraint.

[1]Since constraint (4) computes the expected profit over all representative days, it does not guarantee nonnegative profits at every representative day individually. However, such guarantees could be enforced if constraint (4) were modified as follows: $\sum_{b\in B}\sum_{t\in T} \lambda_{e,t,b} \cdot \left(dis_{e,t,b} \cdot \aleph^{\text{dis}} - ch_{e,t,b}/\aleph^{\text{ch}}\right) \ge 0, \forall e \in E$.

3) Binary constraints on generators ($\forall e \in E, i \in I$):

$$y_{e,t,i} - z_{e,t,i} = v_{e,t,i} - v_{e,t-1,i}, \quad \forall t \in T, \tag{5}$$

$$y_{e,t,i} + z_{e,t,i} \le 1, \quad \forall t \in T, \tag{6}$$

$$v_{e,t,i} = V_{e,i}^0, \quad \forall t \le \overline{L}_{e,i} + \underline{L}_{e,i}, \tag{7}$$

$$\sum_{k=t-UT_i+1}^{t} y_{e,k,i} \le v_{e,t,i}, \quad \forall t \in \left[\overline{L}_{e,i}, n_T\right], \tag{8}$$

$$\sum_{k=t-DT_i+1}^{t} z_{e,k,i} \le 1 - v_{e,t,i}, \quad \forall t \in \left[\underline{L}_{e,i}, n_T\right]. \tag{9}$$

Constraints (5)–(6) implement the binary logic for on/off status, start-up, and shutdown decisions. Constraint (7) accounts for the on/off statuses at the beginning of each day. Constraints (8)–(9) enforce the minimum up and down times.

B. Primal Lower-Level Problem

The objective function of the primal LL (PLL) problem for each representative day e is:

$$\min_{\Xi_{\text{PLL}}} OC_e^{\text{PLL}} := \sum_{t\in T}\sum_{i\in I} c_i^{\text{g}} \cdot g_{e,t,i} + \sum_{t\in T}\sum_{b\in B} VoWS \cdot ws_{e,t,b} + \sum_{t\in T}\sum_{i\in I} \left(c_i^{\text{start}} \cdot y_{e,t,i} + c_i^{\text{nlc}} \cdot v_{e,t,i}\right), \tag{10}$$

where $\Xi_{\text{PLL}} = \left\{ch_{e,t,b}, dis_{e,t,b}, eSoC_{e,t,b}, f_{e,t,l}, g_{e,t,i}, ws_{e,t,b}, \theta_{e,t,b}\right\}$ are the PLL decision variables. The first two terms in (10) account for the incremental cost of generation and the cost of wind spillage. The last term represents the start-up and no-load cost associated with the binary decisions $y_{e,t,i}$ and $v_{e,t,i}$, which are optimized in the UL problem. The PLL constraints are defined as follows (dual variables for each constraint are given in parantheses after a colon):

1) Dispatch constraints ($\forall t \in T, i \in I$): The power output of generators is limited by their minimum and maximum limits (11) and inter-hour ramp rates (12):

$$\underline{G}_i \cdot v_{e,t,i} \le g_{e,t,i} \le \overline{G}_i \cdot v_{e,t,i} : (\underline{\alpha}_{e,t,i}, \overline{\alpha}_{e,t,i}), \tag{11}$$

$$-RD_i \le g_{e,t,i} - g_{e,t-1,i} \le RU_i : (\beta_{e,t,i}^{\text{RD}}, \beta_{e,t,i}^{\text{RU}}). \tag{12}$$

2) DC network constraints ($\forall t \in T, l \in L$): Since this paper considers storage siting and sizing in transmission networks, a meshed topology is assumed. The power flow of each transmission line is calculated in (13) and the power flow limits are enforced in (14):

$$f_{e,t,l} = \frac{\theta_{e,t,o(l)} - \theta_{e,t,r(l)}}{x_l} : (\xi_{e,t,l}), \tag{13}$$

$$-\overline{F}_l \le f_{e,t,l} \le \overline{F}_l : (\underline{\delta}_{e,t,l}, \overline{\delta}_{e,t,l}). \tag{14}$$

3) ES constraints ($\forall t \in T, b \in B$): Constraint (15) computes the ES state-of-charge and constraints (16)–(18) enforce the maximum ES power and energy limits:

$$eSoC_{e,t,b} = eSoC_{e,t-1,b} + ch_{e,t,b} \cdot \Delta\tau - dis_{e,t,b} \cdot \Delta\tau : (\epsilon_{e,t,b}), \tag{15}$$

$$0 \leq ch_{e,t,b} \leq p_b^{\max} : (\underline{\varphi}^{\text{ch}}_{e,t,b}, \overline{\varphi}^{\text{ch}}_{e,t,b}), \tag{16}$$

$$0 \leq dis_{e,t,b} \leq p_b^{\max} : (\underline{\varphi}^{\text{dis}}_{e,t,b}, \overline{\varphi}^{\text{dis}}_{e,t,b}), \tag{17}$$

$$0 \leq eSoC_{e,t,b} \leq eSoC_b^{\max} : (\underline{\varphi}^{\text{eSoC}}_{e,t,b}, \overline{\varphi}^{\text{eSoC}}_{e,t,b}). \tag{18}$$

In (16)–(18), decisions on ES ratings $p_b^{\max}$ and $eSoC_b^{\max}$ are optimized in the UL problem. As in [2], the lower bound in (18) assumes that ES is placed with zero energy charged on the top of its minimum state-of-charge requirement.

4) Nodal power balance ($\forall t \in T, b \in B$): At each bus, the power balance includes the injections from conventional and wind generation, ES, and adjacent transmission lines:

$$\sum_{i \in I_b} g_{e,t,i} - \sum_{l|o(l)=b} f_{e,t,l} + \sum_{l|r(l)=b} f_{e,t,l} + \left(w^{\text{f}}_{e,t,b} - ws_{e,t,b}\right) - ch_{e,t,b}/\aleph^{\text{ch}} + dis_{e,t,b} \cdot \aleph^{\text{dis}} = d_{e,t,b} : (\lambda_{e,t,b}), \tag{19}$$

where the wind spillage is constrained by:

$$0 \leq ws_{e,t,b} \leq w^{\text{f}}_{e,t,b} : (\gamma_{e,t,b}), \tag{20}$$

The wind spillage in eq. (20) is involuntary and is not used for providing active power reserve as explained in [25].

III. Solution Method

The BP (1)–(20) can be recast as a single-level equivalent using a duality-based technique which involves two steps [18], [26]–[29]. First, the primal-dual transformation is applied to the PLL problems due to the convexity of the LL problems (Section III-A). Second, the PLL and the dual LL (DLL) objective functions are equated to enforce the strong duality theorem (Section III-B). The UL and LL decisions are thus simultaneously optimized via the exchange of their decision variables, as depicted in Fig. 1. The nonlinear single-level equivalent of the BP is presented in Section III-C. This nonlinear equivalent is then converted into the single-level MILP problem described in Section III-D using the linearization process shown in Appendix A. Finally, Section III-E summarizes the computational complexity of the single-level MILP problem.

A. Dual Lower-Level Problem

Given the dual variables shown after a colon in (11)–(20), the DLL problem for each representative day e is written as follows:

1) DLL objective function:

$$\begin{aligned}\max_{\Xi_{\text{DLL}}} OC_e^{\text{DLL}} := \sum_{t \in T} \sum_{b \in B} \Big[& \gamma_{e,t,b} \cdot w^{\text{f}}_{e,t,b} + eSoC_b^{\max} \cdot \overline{\varphi}^{\text{eSoC}}_{e,t,b} \\ & + p_b^{\max} \cdot \left(\overline{\varphi}^{\text{ch}}_{e,t,b} + \overline{\varphi}^{\text{dis}}_{e,t,b}\right) + \lambda_{e,t,b} \cdot \left(d_{e,t,b} - w^{\text{f}}_{e,t,b}\right) \Big] \\ & + \sum_{t \in T} \sum_{i \in I} v_{e,t,i} \cdot \left(\overline{\alpha}_{e,t,i} \cdot \overline{G}_i + \underline{\alpha}_{e,t,i} \cdot \underline{G}_i\right) \\ & + \sum_{t \in T} \sum_{i \in I} \left(\beta^{\text{RU}}_{e,t,i} \cdot RU_i - \beta^{\text{RD}}_{e,t,i} \cdot RD_i\right) \\ & + \sum_{i \in I} \left(\beta^{\text{RU}}_{e,1,i} + \beta^{\text{RD}}_{e,1,i}\right) \cdot G^0_{e,i} + \sum_{t \in T} \sum_{l \in L} \left(\overline{\delta}_{e,t,l} - \underline{\delta}_{e,t,l}\right) \cdot \overline{F}_l,\end{aligned} \tag{21}$$

where $\Xi_{\text{DLL}} = \big\{\overline{\alpha}_{e,t,i}, \beta^{\text{RU}}_{e,t,i}, \overline{\delta}_{e,t,l}, \gamma_{e,t,b}, \overline{\varphi}^{\text{eSoC}}_{e,t,b}, \overline{\varphi}^{\text{ch}}_{e,t,b}, \overline{\varphi}^{\text{dis}}_{e,t,b} \leq 0; \underline{\alpha}_{e,t,i}, \beta^{\text{RD}}_{e,t,i}, \underline{\delta}_{e,t,l}, \underline{\varphi}^{\text{eSoC}}_{e,t,b}, \underline{\varphi}^{\text{ch}}_{e,t,b}, \underline{\varphi}^{\text{dis}}_{e,t,b} \geq 0; \lambda_{e,t,b}, \xi_{e,t,l}, \epsilon_{e,t,b}\big\}$ are the DLL decision variables.

2) DLL constraints:

$$\overline{\delta}_{e,t,l} + \underline{\delta}_{e,t,l} + \xi_{e,t,l} - \lambda_{e,t,o(l)} + \lambda_{e,t,r(l)} = 0, \quad \forall t \in T, l \in L, \tag{22}$$

$$\gamma_{e,t,b} - \lambda_{e,t,b} \leq VoWS, \quad \forall t \in T, b \in B, \tag{23}$$

$$\begin{aligned}\overline{\alpha}_{e,t,i} + \underline{\alpha}_{e,t,i} + \beta^{\text{RU}}_{e,t,i} - \beta^{\text{RU}}_{e,t+1,i} + \beta^{\text{RD}}_{e,t,i} - \beta^{\text{RD}}_{e,t+1,i} \\ + \lambda_{e,t,b(i)} = c^{\text{g}}_i, \quad \forall t = 1 \ldots n_T - 1, i \in I,\end{aligned} \tag{24}$$

$$\begin{aligned}\overline{\alpha}_{e,n_T,i} + \underline{\alpha}_{e,n_T,i} + \beta^{\text{RU}}_{e,n_T,i} + \beta^{\text{RD}}_{e,n_T,i} \\ + \lambda_{e,n_T,b(i)} = c^{\text{g}}_i, \quad \forall i \in I,\end{aligned} \tag{25}$$

$$\overline{\varphi}^{\text{ch}}_{e,t,b} + \underline{\varphi}^{\text{ch}}_{e,t,b} - \epsilon_{e,t,b} \cdot \Delta\tau - \lambda_{e,t,b}/\aleph^{\text{ch}} = 0, \quad \forall t \in T, b \in B, \tag{26}$$

$$\overline{\varphi}^{\text{dis}}_{e,t,b} + \underline{\varphi}^{\text{dis}}_{e,t,b} + \epsilon_{e,t,b} \cdot \Delta\tau + \lambda_{e,t,b} \cdot \aleph^{\text{dis}} = 0, \quad \forall t \in T, b \in B, \tag{27}$$

$$\overline{\varphi}^{\text{eSoC}}_{e,t,b} + \underline{\varphi}^{\text{eSoC}}_{e,t,b} + \epsilon_{e,t,b} - \epsilon_{e,t+1,b} = 0, \quad \forall t = 1 \ldots n_T - 1, b \in B, \tag{28}$$

$$\overline{\varphi}^{\text{eSoC}}_{e,n_T,b} + \underline{\varphi}^{\text{eSoC}}_{e,n_T,b} + \epsilon_{e,n_T,b} = 0, \quad \forall b \in B, \tag{29}$$

$$-\sum_{l|o(l)=b} \frac{\xi_{e,t,l}}{x_l} + \sum_{l|r(l)=b} \frac{\xi_{e,t,l}}{x_l} = 0, \forall b \in B, t \in T. \tag{30}$$

B. Strong Duality Condition

For each LL problem and, thus, each representative day e, the strong duality condition is enforced as follows:

$$OC_e^{\text{PLL}} = OC_e^{\text{DLL}} + \sum_{t \in T} \sum_{i \in I} \left(c^{\text{start}}_i \cdot y_{e,t,i} + c^{\text{nlc}}_i \cdot v_{e,t,i}\right). \tag{31}$$

Note that the last term in the right-hand side of (31) offsets the start-up and no-load costs optimized in the UL problem.

C. Nonlinear Single-Level Equivalent

As explained in [18], each LL problem can be replaced by its primal feasibility constraints (11)–(20), its dual feasibility constraints (22)–(30), and the strong duality condition (31). Therefore, the BP (1)–(20) can be recast as a single-level equivalent given by (1)–(9), and $\big\{$(11)–(20), (22)–(31), $\forall e \in E\big\}$. This equivalent is nonlinear because the following nonlinearities appear in the problem: (i) products of continuous DLL ($\lambda_{e,t,b}$) and continuous PLL ($dis_{e,t,b}, ch_{e,t,b}$)

decision variables in the ES profit constraint (4), (ii) products of continuous UL ($eSoC_b^{\max}, p_b^{\max}$) and continuous DLL ($\overline{\varphi}^{\text{eSoC}}_{e,t,b}, \overline{\varphi}^{\text{ch}}_{e,t,b}, \overline{\varphi}^{\text{dis}}_{e,t,b}$) decision variables in (31), and (iii) products of binary UL ($v_{e,t,i}$) and continuous DLL ($\underline{\alpha}_{e,t,i}, \overline{\alpha}_{e,t,i}$) decision variables in (31). These three nonlinearities are converted into equivalent mixed-integer linear expressions as explained in Appendix A.

D. MILP Formulation

Using the linearized expressions from Appendix A, the single-level MILP formulation is given as follows:

$$\text{Eq. (1)}, \tag{32}$$

subject to:

$$\text{Eq. (2)} - \text{(3)}, \text{(5)} - \text{(9)}, \text{(11)} - \text{(20)}, \text{(22)} - \text{(30)}, \tag{33}$$

$$\text{Eq. (A.11)} - \text{(A.13)}, \text{(A.15)} - \text{(A.26)}. \tag{34}$$

In (32)–(34), $\lambda_{e,t,b}$ is modeled as a free variable, which can attain arbitrarily high and low values. In practice, individual market participants may use their market power to influence LMPs and, thus, to maximize their own profit. Therefore, SOs have adopted a set of market power mitigation policies that aim to keep LMPs at a reasonable level to ensure competitive market outcomes [30]. Based on the discussions in [31], [32], the ability of ES to influence LMPs can be limited as ($\forall e \in E, t \in T, b \in B$):

$$(1 - \Delta\lambda) \cdot \bar{\lambda}_{e,t,b} \leq \lambda_{e,t,b} \leq (1 + \Delta\lambda) \cdot \bar{\lambda}_{e,t,b}, \tag{35}$$

where $\Delta\lambda$ is a non-negative parameter regulating the range of deviations of the free variable $\lambda_{e,t,b}$ from the reference values $\bar{\lambda}_{e,t,b}$, which are taken as the LMPs in the case without ES. Given constraint (35), parameter $\Delta\lambda$ can be interpreted as the maximum deviation of the LMPs from the reference value that ES can achieve by exercising market power. The case study presented in Section IV analyzes the sensitivity of the proposed approach to the value of parameter $\Delta\lambda$.

E. Computational Complexity

The single-level equivalent presented in Section III-D is an MILP problem and, therefore, is generally NP-hard. The computational complexity of this problem is characterized by the number of constraints and the number of continuous/binary variables that can be calculated according to Table I. Note that the total number of constraints depends on the initial statuses of conventional generators due to constraints (7)–(9). Hence, Table I provides an upper bound on the number of such constraints.

TABLE I. DIMENSION OF THE SINGLE-LEVEL MILP PROBLEM

# of constraints	$4 + n_E + 3n_B + n_E n_T\left(17n_I + 4n_L + 17n_B + 12n_B n_J\right)$
# of continuous variables	$1 + 2n_B + n_E n_T\left(4n_L + 7n_I + 14n_B + 3n_B n_J\right)$
# of binary variables	$3n_E n_T n_I + n_B n_J$

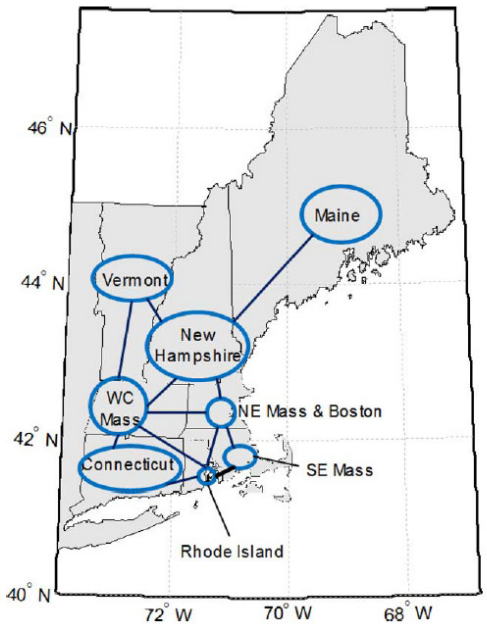

Fig. 2. A diagram of the ISO New England system described in [17].

TABLE II. ZONE NUMBERS FOR THE DIAGRAM IN FIGURE 2

Region	ME	NH	VT	WC Mass	NE Mass	CT	RI	SE Mass
Zone #	1	2	3	4	5	6	7	8

IV. CASE STUDY

A. Test System and Experimental Setup

The single-level MILP problem (32)–(35) was tested using an 8-zone model of the ISO New England system [17]. This test system covering six US states is illustrated in Fig. 2 and includes 76 thermal generators with a total installed capacity of roughly 30 GW. Each zone in this system is numbered in Table II and is modeled as a separate bus in the proposed BP. In addition to generation, load, and transmission data given in [17], annual wind generation profiles with an hourly resolution were taken from [33] for the 30% wind penetration level in terms of annual electricity produced. Given this data and no ES installed, the UC problem is solved for each day of a given year. The resulting annual operating cost is 2544.5 M$. The mean hourly average LMPs at every zone and their standard deviation throughout the year are displayed in Fig. 3. The standard deviation characterizes the range of the LMP distribution over the course of the year and, therefore, gives an indication of LMP variability in each zone.

The recursive hierarchical clustering algorithm described in [34] is used to determine 5 representative days and their respective weights from the year-long demand and wind generation profiles. This algorithm is based on a general-to-specific partitioning approach, which recursively combines daily profiles at every bus in a given number of clusters based on user-defined similarity or dissimilarity metrics. The advantage of this algorithm is that it can simultaneously account for intra-day and seasonal features of these profiles

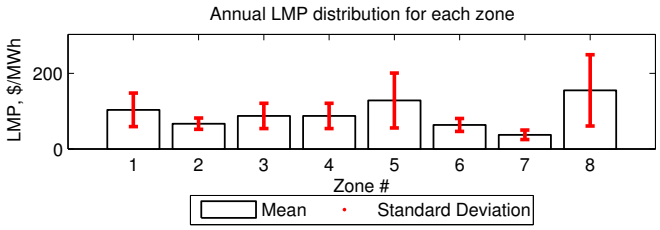

Fig. 3. The mean and standard deviation of hourly LMPs throughout the considered year in case without ES.

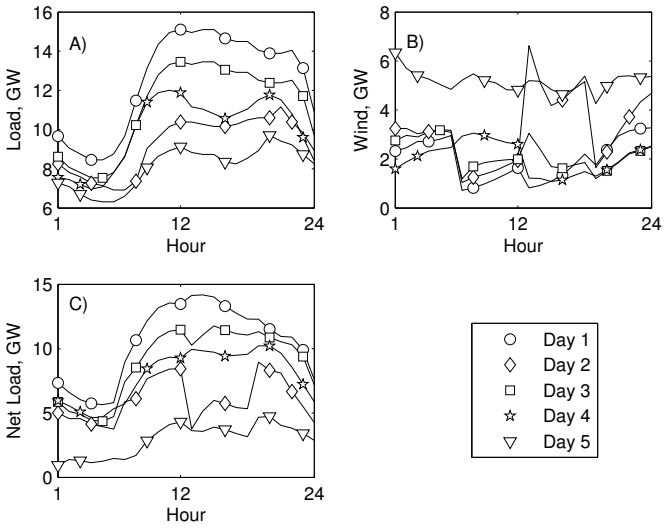

Fig. 4. The system-wide aggregated representative load (A), wind generation (B), and net load (C) profiles. The net load profile is the difference between the load and wind generation profiles.

and has high adaptivity that improves the local data quality. However, other clustering techniques can be applied to obtain representative days. We refer interested readers to [34]–[36] for detailed literature surveys on such techniques. Fig. 4 displays the system-wide aggregated representative load and wind generation profiles for the 5 representative days.

In the following simulations, the value of parameter ρ is set to 6 h, which is a representative energy-to-power ratio for promising ES technologies [1] and sufficient for providing intra-day energy arbitrage [1], [2]. The charging and discharging efficiency of ES are assumed symmetric with $\aleph^{\text{ch}} = \aleph^{\text{dis}} = 0.9$, which also falls within the range of prospective ES technologies [1]. Each ES block is assumed to be $\Delta eSoC$ = 10 MW and the maximum number of blocks in each zone b ($u_b^{\max}$) is set to 300. As in [2], the siting and sizing decisions are analyzed for three capital cost scenarios: low ($20/kWh and $500/kW), medium ($50/kWh and $1000/kW) and high ($75/kWh and $1300/kW). These investment costs are prorated on a daily basis and the values of the c^{p} and c^{eSoC} are obtained for each capital cost scenario assuming that the ES lifetime is 10 years and the annual interest rate is 5%, as explained in [2]. The investment budget is $IC^{\max} = \infty$, i.e., constraint (3) is thus nonbinding, unless stipulated otherwise. Finally, to avoid overestimating the need for ES due to prioritized dispatch of wind generation, the $VoWS$ is set to $0/MWh.

The dimension of the problem for this case study is 3,633,153 constraints, 947,057 continuous variables, and 29,760 binary variables. All simulations were carried out using CPLEX under GAMS 23.7 [37] on an Intel Xenon 2.55 GHz processor with 32 GB of RAM using the Hyak supercomputer system at the University of Washington [38]. The optimality gap was set to 0.1%. All simulations of the proposed BP with different input parameters presented below were completed within 72 hours.

B. Siting and Sizing Decisions

1) Impact of the ES profit constraint (4)*:* Fig. 5 displays the optimized siting and sizing decisions[2] on ES for the low capital cost scenario for different values of χ and $\Delta\lambda$. Regardless of $\Delta\lambda$ chosen, the ES profit constraint (4) affects both the siting and sizing decisions.

If $\Delta\lambda = 0$, i.e., LMPs are not affected by ES installations ($\lambda_{e,t,b} = \bar{\lambda}_{e,t,b}$), siting decisions between the profit-unconstrained ($\chi = 0$) and profit-constrained cases ($\chi = 1$) overlap only in zone 8, which is characterized by the largest variability in LMPs (Fig. 3). However, as $\Delta\lambda$ increases, i.e., ES deployment influences LMPs as compared to the case without ES, the number of shared locations between the profit-constrained and unconstrained cases increases. For instance, if $\Delta\lambda = 0.1$, ES are placed in zones 4 and 8 in both cases. If $\Delta\lambda$ is further increased to 0.2, ES are installed in zones 1, 5 and 8 for both cases.

Regarding the sizing decisions, the profit-unconstrained case consistently results in larger total energy ratings ($\sum_{b\in B} eSoC_b^{\max}$) for any value of $\Delta\lambda$, which also leads to higher investment costs, as illustrated in Fig. 6A. Fig. 6B shows that these decisions do not result in sufficient ES profits to recover such high investment costs, thus leading to net monetary losses, i.e., $\Delta < 0$ (Fig. 6C). Therefore, the profit-unconstrained case overestimates the whole-system need for ES and produces economically nonviable decisions. This conclusion can also be related to the whole-system value of energy storage. As shown in [13], the value of energy storage monotonically reduces as the installed energy storage capacity increases. Thus, larger total energy ratings in the profit-unconstrained cases reduce the whole-system value of storage such that ES owners cannot collect sufficient profits to recover their investment cost.

On the other hand, the profit-constrained decisions have lower total energy ratings and investment costs, resulting in net monetary gain, i.e., $\Delta > 0$ (Fig. 6C). This gain ensures the profitability of ES and economic sustainability of these siting and sizing decisions. This difference between the profit-constrained and unconstrained cases can be attributed to different scheduling priorities. In the profit-unconstrained case, ES are installed and scheduled to minimize the operating cost, so ES are allowed to incur losses if they reduce the operating cost. However, in the profit-constrained case, ES are installed

[2]Recall that the energy and power ratings of ES are assumed to be proportional (A.12). Therefore, the analyses in Section IV-B discuss the sizing decisions in terms of the energy ratings ($eSOC_b^{\max}$).

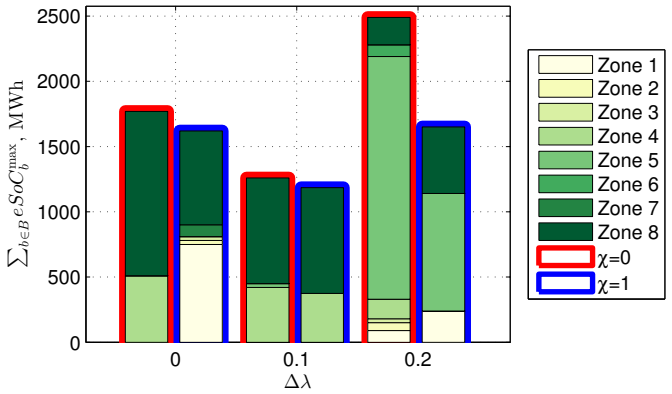

Fig. 5. Effect of the ES profit constraint (4) on the optimized ES siting and sizing decisions for the low capital cost scenario.

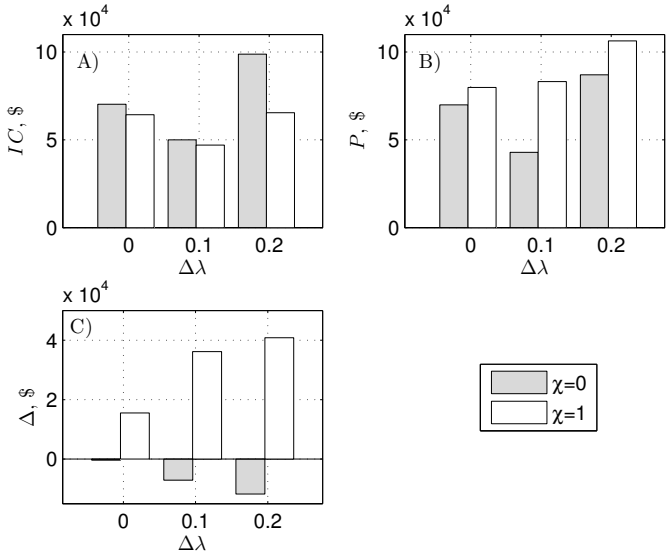

Fig. 6. Effect of the ES profit constraint (4) under the low capital cost scenario on: A) Investment cost of ES (IC), B) expected profit of ES (P), C) net monetary gain/loss of ES ($\Delta = P - IC$).

and scheduled to minimize the system-wide operating cost as long as the investment cost can be fully recovered.

The common thread of the siting decisions in the profit-constrained and unconstrained cases is that ES are usually placed in zones with relatively high variability in LMPs as Fig. 3 shows. This observation is consistent with the empirical siting rule in [39] suggesting that the most likely profit opportunities for ES in a market environment are at buses with the greatest difference between discharging and charging LMPs. Although the variability in LMPs drives the siting decisions, its impact on sizing decisions in the profit-constrained case is not straightforward. For example, Fig. 3 shows that the standard deviation of LMPs is larger in zone 8 than in zone 1, but the ES capacity placed in zone 1 is bigger than in zone 8 for $\Delta\lambda = 0$. Similar observations can be made for zones 4, 5, and 8 in cases with $\Delta\lambda = 0.1$ and $\Delta\lambda = 0.2$.

Figures 6B and 6C show that the regulating parameter $\Delta\lambda$ has a strong correlation with both the ES profit and the recovery of the investment cost, and its effect depends on parameter χ. In the profit-constrained case ($\chi = 1$), increasing $\Delta\lambda$ allows more intra-day variations in LMPs and, thus, the ES profit (Fig. 6B) and the net monetary gain (Fig. 6C) monotonically increases. However, increasing $\Delta\lambda$ would only lead to larger monetary losses in the profit-unconstrained case, i.e., $\chi = 0$ (Fig. 6C).

Since the profit-unconstrained decisions cannot be economically justified, the rest of this paper assumes that $\chi = 1$ and examines the profit-constrained case.

2) Effect of the budget constraint (3)*:* Fig. 7A illustrates the effect of a finite investment budget on the optimized siting and sizing decisions. For tight investment budgets ($IC^{\max} \leq$ \$45000), constraint (3) is binding and there is no diversity in ES allocation and energy ratings for different values of $\Delta\lambda$. ES are systematically placed in zone 8 (highest LMP variability, see Fig. 3) for any value of $\Delta\lambda$. However, as the investment budget increases ($IC^{\max} \geq$ \$60000), Fig. 7A shows that ES are allocated to other zones, resulting in larger total energy ratings. The relationship between the investment cost and the maximum investment budget is shown in Fig. 7B, which distinguishes the cases when the siting and sizing decisions are driven by either the investment budget or the ES profit constraints. When budget constraint (3) is nonbinding, the decisions are driven by the binding profit constraint (4). The large-scale ES deployment needed to accommodate a high penetration of renewable generation [8] requires large investments and would be driven by the profit constraint, thus showing the importance of the proposed planning method.

3) Effect of the operating policy: Profit constraint (4) sums the profits collected by ES in all zones, i.e., it assumes that ES in different zones are operated by the same entity in a *coordinated manner* [15]. In practice ES located in

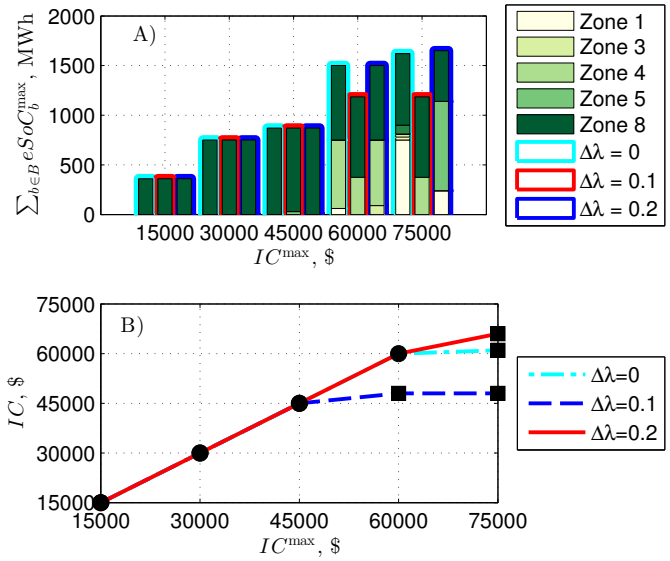

Fig. 7. Effect of the budget constraint (3) under the low capital cost scenario on: A) The optimized ES siting and sizing decisions, B) the relationship between the investment cost and the investment budget. Black circles and squares indicate respectively the cases where the optimization is driven by the binding investment constraint (3) and the ES profit constraint (4).

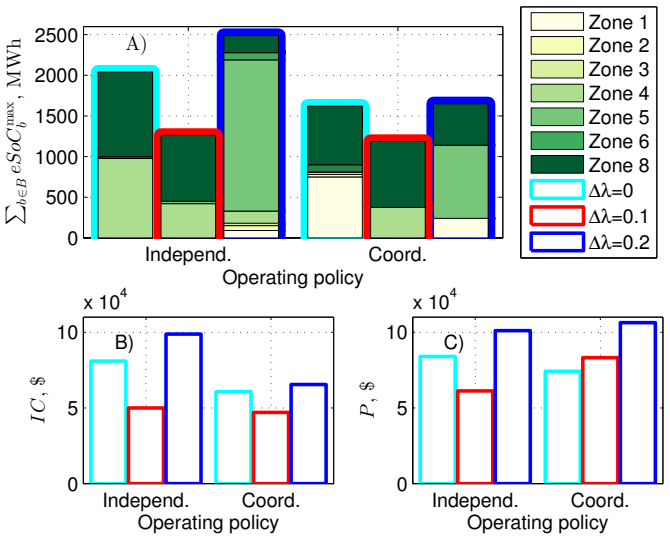

Fig. 8. Effect of the operating policy under the low capital cost scenario on: A) ES siting and sizing decisions, B) investment cost of ES (IC), C) profit of ES (P).

different zones could be operated by *independent* entities. The independent operating policy can be modeled by replacing (4) with nodal ES profit constraints of the following form:

$$\sum_{e\in E}\omega_e\cdot\sum_{t\in T}\lambda_{e,t,b}\cdot\left(dis_{e,t,b}\cdot\aleph^{\text{dis}}-ch_{e,t,b}/\aleph^{\text{ch}}\right)\geq\chi\cdot IC,\quad\forall b\in B. \tag{36}$$

Fig. 8A illustrates the difference between ES siting and sizing decisions with the coordinated and independent operating policies. As compared to the independent policy, the coordinated policy consistently results in lower total ES ratings and, thus, it requires lower investments (Fig. 8B). On the other hand, despite the lower total ES ratings, the coordinated policy results in higher profits than the independent policy for $\Delta\lambda>0$. Hence, an ES block installed under the coordinated policy is utilized more efficiently than under the independent policy when ES deployment influences the LMPs as compared to the case without ES.

4) Impact of the capital cost: If the capital cost increases, the ES are allocated at fewer zones and their total energy rating decreases, as shown in Fig. 9 for the coordinated operating policy. Under the high capital cost scenario, ES are only placed at zone 8. Furthermore, there is a relatively small difference between the energy ratings for different values of $\Delta\lambda$. This observation suggests that as long as the capital cost of ES remains prohibitively expensive, the ability of ES to influence LMPs is insignificant due to their relatively low penetration. However, provided the anticipated ES capital cost reduction, accounting for impacts of ES on LMPs would be of greater value.

C. Evaluation of Costs and Profits

To assess the performance of the system with the various siting and sizing decisions made as explained above, the UC problem is solved for each day of a given year. This assessment

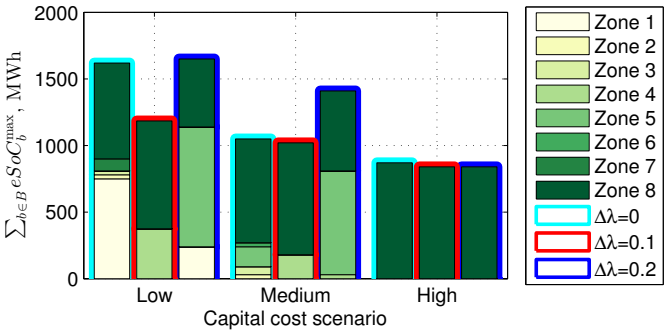

Fig. 9. Effect of the capital cost on the profit-constrained ES siting and sizing decisions under the coordinated policy.

TABLE III. ANNUAL ASSESSMENT OF THE ES SITING AND SIZING DECISIONS FOR DIFFERENT OPERATING POLICIES AND VALUES OF $\Delta\lambda$

Metric	Operating policy	$\Delta\lambda$ 0	0.1	0.2
$\overline{OC}^{SO}$, M$	Coordinated	2,439.7	2,449.8	2,455.0
	Independent	2,439.9	2,457.8	2,461.3
$\overline{CS}^{SO}$, M$	Coordinated	104.8	94.6	89.2
	Independent	104.6	86.7	83.2
$\overline{P}^{ES}$, M$	Coordinated	267.6	275.8	286.5
	Independent	234.1	239.1	247.2
$\overline{WS}$, MWh	Coordinated	51.5	52.1	52.7
	Independent	98.7	96.4	96.1

TABLE IV. ANNUAL ASSESSMENT OF THE ES SITING AND SIZING DECISIONS FOR DIFFERENT CAPITAL COSTS AND VALUES OF $\Delta\lambda$

Metric	Capital cost	$\Delta\lambda$ 0	0.1	0.2
$\overline{OC}^{SO}$, M$	Low	2,439.7	2,449.8	2,455.0
	Medium	2,480.4	2,486.4	2,488.9
	High	2,491.3	2,495.4	2,495.8
$\overline{CS}^{SO}$, M$	Low	104.8	94.6	89.2
	Medium	64.1	58.1	55.6
	High	53.2	49.1	48.7
$\overline{P}^{ES}$, M$	Low	267.6	275.8	286.5
	Medium	216.7	241.2	247.4
	High	209.3	216.2	216.2
$\overline{WS}$, MWh	Low	51.5	52.1	52.7
	Medium	64.7	70.5	79.2
	High	87.4	101.4	101.4

is based on the following metrics: Average daily operating cost for the SO ($\overline{OC}^{SO}$), average daily cost savings for the SO ($\overline{CS}^{SO}$) relative to the case without ES, average daily profit for the ES ($\overline{P}^{ES}$), and average daily wind spillage ($\overline{WS}$).

Table III presents the evaluation of the profit-constrained ES siting and sizing decisions made without budget limits and for the low capital cost scenario. It shows that the coordinated operating policy of ES leads to lower annual operating costs and larger annual cost savings for the SO than the independent operating policy. Similarly, the coordinated operating policy results in larger ES profits. Both the ES and SO metrics are sensitive to the value of $\Delta\lambda$. As $\Delta\lambda$ increases, which translates into larger influence of ES on LMPs, the annual profit of the ES increases. This increase in ES profits comes at the expense of an increase in the annual operating cost and, thus, reduces

the annual cost savings for the SO. The coordinated operating policy reduces the annual wind spillage by a factor of two as compared to the independent operating policy. Notably, parameter $\Delta\lambda$ marginally affects the annual wind spillage for a given policy.

Table IV presents the evaluation of the profit-constrained ES siting and sizing decisions made without budget limits with the coordinated operating policy under different capital cost scenarios. As in Table III, all metrics are sensitive to $\Delta\lambda$. However, this sensitivity varies with the capital cost. As the capital cost increases, the difference in cost savings between cases with $\Delta\lambda = 0$ and $\Delta\lambda = 0.2$ reduces. Similarly, the difference in ES profits between those cases non-monotonically decreases. Thus, the ES ability to influence LMPs would chiefly affect the ES profit and SO savings when the ES capital cost is lower. If the capital cost is relatively high, the influence of ES on LMPs would have a moderate impact on these metrics. Also, as the capital cost decreases, more ES capacity is installed, which leads to lower annual wind spillage.

V. Conclusion

This paper presents a bilevel program for optimally siting and sizing ES that accounts for the perspectives of both the SO and the owners of ES devices. The results indicate that the optimal ES siting and sizing decisions are sensitive to the minimum profit constraint. This constraint represents a linear relationship between the short-term operational profit and long-term investment cost of merchant ES. If the profitability requirement is not accounted for, i.e. parameter χ is set to 0, ES owners would not be able to recover their investment costs, leading to economically nonviable siting and sizing decisions. The case study also reveals the sensitivity of the profit-constrained siting and sizing decisions to:

- Operating policy: Enabling coordinated ES operations at different buses increases ES profits and SO cost savings, as well as reduces wind spillage;
- Ability to influence LMPs: Merchant ES can extract additional profits by influencing LMPs, which comes at the expense of a larger system-wide operating cost;
- Capital cost: As the capital cost of ES remains prohibitively expensive, ES cannot take advantage of the coordinated operating strategy and influencing LMPs.

The work in this manuscript points to several areas for potential future work:

- Improving computational tractability of the proposed mathematical framework with decomposition solution techniques to achieve scalability for larger transmission networks.
- Incorporating other potential profit streams, such as reserve provision and capacity market payments.
- The investment model merits further theoretical research to accommodate multiple decision-making stages, i.e., a so-called dynamic approach.
- The proposed approach can be used for deriving ad-hoc siting and sizing rules to provide "warm start" solutions for more complex and computationally challenging siting and sizing models.

Acknowledgment

The authors thank Dr. Gyuk and his colleagues at the US DOE Energy Storage Program for funding this research. Sandia National Laboratories is a multi-program laboratory managed and operated by Sandia Corporation, a wholly owned subsidiary of Lockheed Martin Corporation, for the U.S. Department of Energy's National Nuclear Security Administration under Contract DE-AC04-94AL85000.

Appendix A
Linearization of the Nonlinear Single-Level Equivalent

1) Linearization of the ES profit constraint (4)*:* The ES profit in (4) can be equivalently expressed in terms of other dual variables in order to linearize it using the complementary slackness conditions of each LL problem. First, using (III-A2) and (27), the ES profit in (4) for each representative day e results in:

$$\sum_{t\in T}\sum_{b\in B}\lambda_{e,t,b}\cdot\left(dis_{e,t,b}\cdot\aleph^{\text{dis}}-ch_{e,t,b}/\aleph^{\text{ch}}\right)= \sum_{t\in T}\sum_{b\in B}\Big[\epsilon_{e,t,b}\cdot\Delta\tau\cdot(ch_{e,t,b}-dis_{e,t,b})- dis_{e,t,b}\cdot\left(\underline{\varphi}^{\text{dis}}_{e,t,b}+\overline{\varphi}^{\text{dis}}_{e,t,b}\right)-ch_{e,t,b}\cdot\left(\underline{\varphi}^{\text{ch}}_{e,t,b}+\overline{\varphi}^{\text{ch}}_{e,t,b}\right)\Big]. \quad \text{(A.1)}$$

Expressing $\Delta\tau\cdot(ch_{e,t,b}-dis_{e,t,b})$ in terms of $eSoC_{e,t,b}$ from (15), the first term in the right-hand side of (A.1), hereinafter denoted as $\mathcal{K}_e$, can be expressed as:

$$\mathcal{K}_e=\sum_{t\in T}\sum_{b\in B}\epsilon_{e,t,b}\cdot(eSoC_{e,t,b}-eSoC_{e,t-1,b}). \quad \text{(A.2)}$$

The terms in the right-hand side of (A.2) can be rearranged as:

$$\mathcal{K}_e=\sum_{t=1}^{n_T-1}\sum_{b\in B}eSoC_{e,t,b}\cdot\left(\epsilon_{e,t,b}-\epsilon_{e,t+1,b}\right)+\sum_{b\in B}eSoC_{e,n_T,b}\cdot\epsilon_{e,n_T,b}. \quad \text{(A.3)}$$

Equation (A.3) can be equivalently expressed in terms of $\overline{\varphi}^{\text{eSoC}}_{e,t,b}$ and $\underline{\varphi}^{\text{eSoC}}_{e,t,b}$ from (28) and (29) as:

$$\mathcal{K}_e=\sum_{t\in T}\sum_{b\in B}eSoC_{e,t,b}\cdot\left(-\underline{\varphi}^{\text{eSoC}}_{e,t,b}-\overline{\varphi}^{\text{eSoC}}_{e,t,b}\right). \quad \text{(A.4)}$$

The first term in the right-hand side of (A.1) can be replaced with (A.4), thus equivalently reformulating (A.1) as follows:

$$\sum_{t\in T}\sum_{b\in B}\lambda_{e,t,b}\cdot(dis_{e,t,b}\cdot\aleph^{\text{dis}}-ch_{e,t,b}/\aleph^{\text{ch}})= -\sum_{t\in T}\sum_{b\in B}\Big[eSoC_{e,t,b}\cdot(\underline{\varphi}^{\text{eSoC}}_{e,t,b}+\overline{\varphi}^{\text{eSoC}}_{e,t,b})+ dis_{e,t,b}\cdot(\underline{\varphi}^{\text{dis}}_{e,t,b}+\overline{\varphi}^{\text{dis}}_{e,t,b})+ch_{e,t,b}\cdot(\underline{\varphi}^{\text{ch}}_{e,t,b}+\overline{\varphi}^{\text{ch}}_{e,t,b})\Big]. \quad \text{(A.5)}$$

The following equalities can be derived using the complementary slackness conditions associated with constraints (16)–(18), $\forall t\in T, b\in B$:

$$dis_{e,t,b} \cdot \overline{\varphi}^{\text{dis}}_{e,t,b} = p^{\max}_{b} \cdot \overline{\varphi}^{\text{dis}}_{e,t,b}, \tag{A.6}$$

$$ch_{e,t,b} \cdot \overline{\varphi}^{\text{ch}}_{e,t,b} = p^{\max}_{b} \cdot \overline{\varphi}^{\text{ch}}_{e,t,b}, \tag{A.7}$$

$$eSoC_{e,t,b} \cdot \overline{\varphi}^{\text{eSoC}}_{e,t,b} = eSoC^{\max}_{b} \cdot \overline{\varphi}^{\text{eSoC}}_{e,t,b}, \tag{A.8}$$

$$ch_{e,t,b} \cdot \underline{\varphi}^{\text{ch}}_{e,t,b} = dis_{e,t,b} \cdot \underline{\varphi}^{\text{dis}}_{e,t,b} = eSoC_{e,t,b} \cdot \underline{\varphi}^{\text{eSoC}}_{e,t,b} = 0. \tag{A.9}$$

After using the equalities (A.6)–(A.9) for the nonlinear terms in (A.5), the ES profits are equivalently rewritten as a nonlinear function depending on the ES power and energy ratings:

$$\sum_{t\in T}\sum_{b\in B} \lambda_{e,t,b} \cdot \left(dis_{e,t,b} \cdot \aleph^{\text{dis}} - ch_{e,t,b}/\aleph^{\text{ch}}\right) = -\sum_{t\in T}\sum_{b\in B} \left[eSoC^{\max}_{b} \cdot \overline{\varphi}^{\text{eSoC}}_{e,t,b} + p^{\max}_{b} \cdot \left(\overline{\varphi}^{\text{ch}}_{e,t,b} + \overline{\varphi}^{\text{dis}}_{e,t,b)}\right)\right]. \tag{A.10}$$

To equivalently reformulate (A.10) as a linear expression, ES ratings are modeled as:

$$eSoC^{\max}_{b} = \sum_{j\in J} \Delta eSOC \cdot u_{b,j}, \forall b \in B \tag{A.11}$$

$$p^{\max}_{b} = eSoC^{\max}_{b} \cdot \rho^{-1} = \sum_{j\in J} \Delta eSOC \cdot \rho^{-1} \cdot u_{b,j}, \forall b \in B \tag{A.12}$$

$$\sum_{j\in J} u_{b,j} \leq u^{\max}_{b}, \forall b \in B. \tag{A.13}$$

In (A.11) and (A.12), we assume that at every bus ES is assembled from standard blocks that have fixed energy ($\Delta eSOC$) and power ($\Delta eSOC \cdot \rho^{-1}$) ratings. For instance, the ratio between these energy and power ratings is assumed constant [2] and the coefficient ρ depends on the storage technology [12]. Constraint (A.13) limits the number of blocks that can be installed at each bus. Using (A.11) and (A.12), the ES profits (A.10) can be equivalently reformulated as:

$$\sum_{t\in T}\sum_{b\in B} \lambda_{e,t,b} \cdot \left(dis_{e,t,b} \cdot \aleph^{dis} - ch_{e,t,b}/\aleph^{ch}\right) = -\sum_{t\in T}\sum_{b\in B}\sum_{j\in J} \Delta eSoC \cdot u_{b,j} \cdot \left(\overline{\varphi}^{\text{eSoC}}_{e,t,b} + \rho^{-1} \cdot \left(\overline{\varphi}^{\text{ch}}_{e,t,b} + \overline{\varphi}^{\text{dis}}_{e,t,b}\right)\right). \tag{A.14}$$

Expression (A.14) still contains three products of binary and continuous variables that are linearized using the 'big M' method [29]. This linearization comes at the expense of auxiliary continuous variables ($a^{1}_{e,t,b,j}$ and $a^{2,\text{ch/dis}}_{e,t,b,j}$) and constraints (A.16)–(A.21). Constraint (4) is replaced with the following equivalent:

$$-\sum_{e\in E} \omega_e \sum_{t\in T}\sum_{b\in B}\sum_{j\in J} \left(a^{1}_{e,t,b,j} + a^{2,\text{ch}}_{e,t,b,j} + a^{2,\text{dis}}_{e,t,b,j}\right) \geq \chi \cdot IC, \tag{A.15}$$

and the linear constraints ($\forall e \in E, t \in T, b \in B, j \in J$):

$$-M \cdot (1 - u_{b,j}) \leq \overline{\varphi}^{\text{eSoC}}_{e,t,b} \cdot \Delta eSoC - a^{1}_{e,t,b,j} \leq 0, \tag{A.16}$$

$$-M \cdot (1 - u_{b,j}) \leq \overline{\varphi}^{\text{ch}}_{e,t,b} \cdot \rho^{-1} \cdot \Delta eSoC - a^{2,\text{ch}}_{e,t,b,j} \leq 0, \tag{A.17}$$

$$-M \cdot (1 - u_{b,j}) \leq \overline{\varphi}^{\text{dis}}_{e,t,b} \cdot \rho^{-1} \cdot \Delta eSoC - a^{2,\text{dis}}_{e,t,b,j} \leq 0, \tag{A.18}$$

$$-M \cdot u_{b,j} \leq a^{1}_{e,t,b,j} \leq 0, \tag{A.19}$$

$$-M \cdot u_{b,j} \leq a^{2,\text{ch}}_{e,t,b,j} \leq 0, \tag{A.20}$$

$$-M \cdot u_{b,j} \leq a^{2,\text{dis}}_{e,t,b,j} \leq 0. \tag{A.21}$$

Since the linearization process presented in this subsection is based on algebraic manipulations, complementary slackness conditions, and the 'big M' method, the left-hand side in (A.15) is an exact equivalent of the left-hand side in (4). Therefore, this linearization does not affect the accuracy of the solution.

2) Linearization of the strong duality equality (31)*:* As shown in (21), the term OC^{DLL}_{e} in (31) contains several nonlinear terms. The second and third terms in (21) are identical to the right-hand side of (A.10) and, thus, the same linearization technique can be applied. The fifth term in (21) involving the products $v_{e,t,i} \cdot \overline{\alpha}_{e,t,i} \cdot \overline{G}_i$ and $v_{e,t,i} \cdot \underline{\alpha}_{e,t,i} \cdot \underline{G}_i$ can also be linearized using the 'big M' method [29]. Therefore, constraint (31) is replaced for each representative day e with:

$$OC^{\text{PLL}}_{e} = \sum_{t\in T}\sum_{b\in B} \Big[\gamma_{e,t,b} \cdot w^{\text{f}}_{e,t,b} + \lambda_{e,t,b} \cdot \left(d_{e,t,b} - w^{\text{f}}_{e,t,b}\right) + \sum_{j\in J} \left(a^{1}_{e,t,b,j} + a^{2,\text{ch}}_{e,t,b,j} + a^{2,\text{dis}}_{e,t,b,j}\right)\Big] + \sum_{t\in T}\sum_{i\in I} \Big[\overline{h}_{e,t,i} + \underline{h}_{e,t,i} + \beta^{\text{RU}}_{e,t,i} \cdot RU_i - \beta^{\text{RD}}_{e,t,i} \cdot RD_i + c^{\text{start}}_{i} \cdot y_{e,t,i} + c^{\text{nlc}}_{i} \cdot v_{e,t,i}\Big] + \sum_{i\in I} \left(\beta^{\text{RU}}_{e,1,i} + \beta^{\text{RD}}_{e,1,i}\right) \cdot G^{0}_{e,i} + \sum_{t\in T}\sum_{l\in L} \left(\overline{\delta}_{e,t,l} - \underline{\delta}_{e,t,l}\right) \cdot \overline{F}_l, \tag{A.22}$$

$$-M \cdot (1 - v_{e,t,i}) \leq \overline{\alpha}_{e,t,i} \cdot \overline{G}_i - \overline{h}_{e,t,i} \leq 0, \forall t \in T, i \in I, \tag{A.23}$$

$$0 \leq \underline{\alpha}_{e,t,i} \cdot \underline{G}_i - \underline{h}_{e,t,i} \leq M \cdot (1 - v_{e,t,i}), \forall t \in T, i \in I, \tag{A.24}$$

$$-M \cdot v_{e,t,i} \leq \overline{h}_{e,t,i} \leq 0, \forall t \in T, i \in I, \tag{A.25}$$

$$0 \leq \underline{h}_{e,t,i} \leq M \cdot v_{e,t,i}, \forall t \in T, i \in I. \tag{A.26}$$

The proposed linearization scheme relies on the 'big M' method and, thus, requires setting bounds on LL dual variables, which are known as the 'big M' values. The computational performance of the BP can be affected by the selections of the 'big M' values, especially when implemented for large-scale systems. This drawback could be overcome either by appropriately selecting the big-M values or avoiding the use of the 'big M' method [40], [41].

REFERENCES

[1] B. Dunn, H. Kamath, and J.-M. Tarascon, "Electrical energy storage for the grid: A battery of choices," *Science*, vol. 334, pp. 928–935, 2011.

[2] H. Pandžić, Y. Wang, T. Qiu, Y. Dvorkin, and D.S. Kirschen, "Near-optimal method for siting and sizing of distributed storage in a transmission network," *IEEE Trans. Power Syst.*, vol. 30, no. 5, pp. 2288–2300, Sep. 2015.

[3] D. Gayme and U. Topcu, "Optimal power flow with large-scale storage integration," *IEEE Trans. Power Syst.*, vol. 28, no. 2, pp. 709–717, 2013.

[4] Y. V. Makarov, P. Du, M. C. W. Kintner-Meyer, C. Jin, and H. F. Illian, "Sizing energy storage to accommodate high penetration of variable energy resources," *IEEE Trans. Power Syst.*, vol. 3, no. 1, pp. 34–40, 2012.

[5] B. M. Grainger, G. Reed, A.R. Sparacino, and P.T. Lewis, "Power electronics for grid-scale energy storage," *Proceedings of the IEEE*, vol. 102, no. 6, pp. 1000–1013, 2014.

[6] L. S. Vargas, G. Bustos-Turu, and F. Larrain, "Wind power curtailment and energy storage in transmission congestion management considering power plants ramp rates," *IEEE Trans. Power Syst.*, vol. 30, no. 5, pp. 2498–2506, 2015.

[7] Y. Dvorkin, M. Lubin, S. Backhaus, M. Chertkov, "Uncertainty Sets for Wind Power Generation," *IEEE Transactions on Power Systems*, early access, 2016.

[8] A. A. Solomon, D. M. Kammen, and D. Callaway, "The role of large-scale energy storage design and dispatch in the power grid," *Appl. Energy*, vol. 134, pp. 75–89, 2014.

[9] M. C. W. Kintner-Meyer, P. J. Balducci, V. V. Viswanathan, C. Jin, X. Guo, T. B. Nguyen, and F. K. Tuffner, "Energy storage for power systems applications: A regional assessment for the Northwest Power Pool," Technical report, 2010. [Online]. Available at: http://www.pnl.gov/main/publications/external/technical_reports/PNNL-19300.pdf

[10] "Advancing and maximizing the value of energy storage technology," Technical report, 2014. [Online]. Available at: http://www.caiso.com/documents/advancing-maximizingvalueofenergy storagetechnology_californiaroadmap.pdf

[11] Federal Energy Regulatory Commission (FERC) Order No. 792, "Small Generator Interconnection Agreements and Procedures". [Online]. Available at: https://www.ferc.gov/whats-new/comm-meet/2013/112113/E-1.pdf

[12] S. Wogrin and D. F. Gayme, "Optimizing storage siting, sizing, and technology portfolios in transmission-constrained networks," *IEEE Trans. Power Syst.*, vol. 30, no. 6, pp. 3304–3313, Nov. 2015.

[13] D. Pudjianto, M. Aunedi, P. Djapic, and G. Strbac, "Whole-systems assessment of the value of energy storage in low-carbon electricity systems," *IEEE Trans. Smart Grid*, vol. 5, no. 2, pp. 1098–1109, Mar. 2014.

[14] K. Dvijotham, M. Chertkov, and S. Backhaus, "Storage sizing and placement through operational and uncertainty-aware simulations," in Proceedings of the *47th Hawaii International Conference on Systems Science*, pp. 2408–2416, 2014.

[15] H. Mohsenian-Rad, "Coordinated price-maker operation of large energy storage units in nodal energy markets," *IEEE Trans. Power Syst.*, vol. 31, no. 1, pp. 786–797, Jan. 2016.

[16] A. Castillo and D. F. Gayme, "Profit maximizing storage allocation in power grids," in Proc. of the *2013 IEEE 52nd Annual Conferences on Decision and Control*, pp. 429–435, 2014.

[17] D. Krishnamurthy, W. Li, and L. Tesfatsion, "An 8-zone test system based on ISO New England data: Development and application," *IEEE Trans. Power Syst.*, vol. 31, no. 1, pp. 234–246, Jan. 2016.

[18] J. M. Arroyo, "Bilevel programming applied to power system vulnerability analysis under multiple contingencies," *IET Gener. Transm. Distrib.*, vol. 4, pp. 178–190, 2010.

[19] L. P. Garces, A. J. Conejo, R. García-Bertrand, and R. Romero "A Bilevel approach to transmission expansion planning within a market environment," *IEEE Trans. Power Syst.*, vol. 24, no.3, pp. 1513–1522, Aug. 2009.

[20] R. Fernández-Blanco, J. M. Arroyo, and N. Alguacil, "A unified bilevel programming framework for price-based market clearing under marginal pricing," *IEEE Trans. Power Syst.*, vol. 27, no. 1, pp. 517–525, Feb. 2012.

[21] S. A. Gabriel, A. J. Conejo, D. Fuller, B. F. Hobbs, and C. Ruiz, "Complementarity Modeling in Energy Markets," *Springer: International Series in Operation Research & Management Science*, New York, USA, 2012.

[22] L. Baringo and A. J. Conejo, "Strategic wind power investment," *IEEE Trans. Power Syst.*, vol. 29, no. 3, pp. 1250–1260, May 2014.

[23] S. Tegen, E. Lantz, M. Hand, B. Maples, A. Smith, and P. Schwabe, "2011 Cost of Wind Energy: Review," National Renewable Energy Laboratory, 2011. [Online]. Available at: http://www.nrel.gov/docs/fy13osti/56266.pdf

[24] P. D. Easton, "PE ratios, PEG ratios, and estimating the implied expected rate of return on equity capital," *The Accounting Review*, vol. 79, no. 1, pp. 73–95, Jan. 2004.

[25] Y. Dvorkin, M.A. Ortega-Vazuqez, D.S. Kirschen, "Wind generation as a reserve provider," *IET Generation, Transmission & Distribution*, vol.9, no.8, pp. 779-787.

[26] A. L. Motto, J. M. Arroyo, and F. D. Galiana, "A mixed-integer LP procedure for the analysis of electric grid security under disruptive threat," *IEEE Trans. Power Syst.*, vol. 20, no. 3, pp. 1357–1365, Aug. 2005.

[27] C. Ruiz and A. Conejo, "Pool strategy of a producer with endogenous formation of LMPs," *IEEE Trans. Power Syst.*, vol. 24, no. 4, pp. 855–866, Nov. 2009.

[28] R. Fernández-Blanco, J. M. Arroyo, and N. Alguacil, "Bilevel programming for price-based electricity auctions: A revenue-constrained case," *EURO J. Comput. Optim.*, vol. 3, no. 3, pp. 163–195, Apr. 2015.

[29] C. A. Floudas, *Nonlinear and Mixed-Integer Optimization: Fundamentals and Applications*. New York, NY, USA: Oxford University Press, 1995.

[30] Federal Energy Regulatory Commission (FERC), "Price Formation in Organized Wholesale Electricity Markets: Staff Analysis of Energy Offer Mitigation in RTO and ISO Markets," 2014. [Online]. Available at: https://www.ferc.gov/legal/staff-reports/2014/AD14-14-mitigation-rto-iso-markets.pdf

[31] R. O'Neill, D. Mead, and P. Malvadkar, "On market clearing prices higher than the highest bid and other almost paranormal phenomena," *The Electricity Journal*, vol. 18, no. 2, pp. 19–27, Mar. 2005.

[32] F. Wolak, "Diagnosing the California electricity crisis," *The Electricity Journal*, vol. 16, no. 7, pp. 11–37, Aug.-Sep. 2003.

[33] Eastern Wind Dataset, *National Renewable Energy Laboratory*, 2012. [Online]. Available at: http://www.nrel.gov/electricity/transmission/eastern_wind_methodology.html

[34] B. Pitt, "Applications of data mining techniques to electric load profiling", *PhD thesis*, University of Manchester, UK, 2000. [Online]. Available at: http://www.ee.washington.edu/research/real/Library/Thesis/Barnaby_PITT.pdf

[35] S. Wogrin, D. Galbally, and J. Reneses, "Optimizing storage operations in medium- and long-term power system models," *IEEE Trans. Power Syst.*, early access, pp.1–10, 2015.

[36] D. Getman, A. Lopez, T. Mai, and M. Dyson, "Methodology for Clustering High-Resolution Spatiotemporal Solar Resource Data," Technical report, 2015. [Online]. Available at: http://www.nrel.gov/docs/fy15osti/63148.pdf

[37] R. E. Rosenthal, "GAMS – A Users Guide", GAMS Corp., 2013.

[38] Hyak Supercomputer, 2015. [Online]. Available at: http://escience.washington.edu/content/hyak-0

[39] V. Krishnan and T. Das, "Optimal allocation of energy storage in a co-optimized electricity market: Benefits assessment and deriving indicators for economic storage ventures", *Energy*, vol. 815, pp. 175–188, Mar. 2015.

[40] J. F. Bard and J. T. Moore, "A branch and bound algorithm for the bilevel programming problem," *SIAM J. Sci. Statist. Comput.*, vol. 11, no. 2, pp. 281–292, 1990.

[41] J. Hu, J. E. Mitchell, J.-S. Pang, K. P. Bennett, and G. Kunapuli, "On the global solution of linear programs with linear complementarity constraints," *SIAM J. Optim.*, vol. 19, no. 1, pp. 445–471, 2008.

Yury Dvorkin (S'11) received the B.S.E.E degree with the highest honors at Moscow Power Engineering Institute (Technical University), Moscow, Russia, in 2011. He is currently pursuing the Ph.D. degree in electrical engineering at the University of Washington, Seattle, WA, USA. His research interests include short- and long-term planning in power systems with renewable generation and power system economics.

Ricardo Fernández-Blanco (S'10-M'15) received the Ingeniero Industrial degree and the Ph.D. degree in electrical engineering from the Universidad de Castilla-La Mancha, Ciudad Real, Spain, in 2009 and 2014, respectively.

He is currently a Post-doctoral Researcher at University of Washington, Seattle, WA, USA. His research interests are in the fields of operations and economics of power systems, bilevel programming, and electricity markets.

Daniel S. Kirschen (M'86-SM'91-F'07) received the degree in electrical and mechanical engineering from the Universite Libre de Bruxelles, Brussels, Belgium, and the M.Sc. and Ph.D. degrees from the University of Wisconsin, Madison, WI, USA, 1979, 1980, and 1985, respectively.

He is currently a Close Professor of Electrical Engineering with the University of Washington, Seattle, WA, USA. His research interests include smart grids, the integration of renewable energy sources in the grid, power system economics, and power system security.

Hrvoje Pandžić (S'06-M'12) received the M.E.E. and Ph.D. degrees from the Faculty of Electrical Engineering and Computing, University of Zagreb, Zagreb, Croatia, in 2007 and 2011, respectively. From 2012 to 2014, he was a Postdoctoral Researcher with the University of Washington, Seattle, WA, USA.

Currently, he is an Assistant Professor with the Faculty of Electrical Engineering and Computing, University of Zagreb. His research interests include planning, operation, control, and economics of power and energy systems.

Jean-Paul Watson (M'10) received the B.S., M.S., and Ph.D. degrees in computer science.

He is a Distinguished Member of Technical Staff with the Discrete Math and Optimization Department, Sandia National Laboratories, Albuquerque, NM, USA. He leads a number of research efforts related to stochastic optimization, ranging from fundamental algorithm research and development, to applications including power grid operations and planning.

Cesar A. Silva-Monroy (M'15) received the B.S. degree from the Universidad Industrial de Santander, Bucaramanga, Colombia, and the M.S. and Ph.D. degrees from University of Washington, Seattle, WA, USA, all in electrical engineering.

He is a Senior Member of Technical Staff with Sandia National Laboratories, Albuquerque, NM, USA. He currently leads projects on electric grid resilience, planning and operations. His research interests also include electricity markets and renewable energy integration